

Homogeneous, Coaxial Liquid Crystal Domain Growth from Carbon Nanotube Seeds

Randy A. Mrozek, Byeong-Su Kim, Vincent C. Holmberg, and T. Andrew Taton*

Department of Chemistry, University of Minnesota, 207 Pleasant Street SE, Minneapolis, Minnesota 55455

Received September 14, 2003; Revised Manuscript Received October 7, 2003

ABSTRACT

We have developed a general method for aligning anisotropic materials by using carbon nanotubes to influence order in the surrounding material. Specifically, we have shown that carbon nanotubes seed the formation of oriented domains in a liquid crystalline polymer (LCP). Using polarized light microscopy, we have observed that the molecular alignment in these large (10–100 μm long) domains is homogeneous and controlled by the direction of the nanotube nucleus. The kinetic nature of this nucleation process was verified by differential scanning calorimetry. The coupling of preferential nucleation and controlled seed orientation may allow bulk LCP materials to be aligned by simply preorganizing a small number of dispersed nanotube seeds. We expect that this work will aid in the development and application of macroscopically ordered nanostructured composite materials.

Liquid crystalline polymers (LCPs) have become increasingly important in materials engineering because of their unique electrical, optical, and mechanical properties.¹ The properties of LCPs can be highly anisotropic, depending on the degree of molecular or supramolecular alignment present in micron-sized, liquid-crystalline (LC) domains.² Optimizing both LCP properties and anisotropy requires that the orientation and growth of individual domains be closely controlled. For example, homogeneous alignment of LC domains in aramid or polyester fiber and film dramatically improves the tensile strength and modulus of these materials.^{3,4} Alignment of LCP domains is typically controlled by shear during processing,^{5,6} but can also be affected by applied electric⁷ or magnetic⁸ fields, or by contact with a structured surface.^{9,10} In this report we describe an alternative technique for controlling the organization of LCP domains, in which small quantities of single-walled carbon nanotubes (SWNTs) are dispersed in the material and serve as seeds for oriented domain growth from the isotropic melt. The resulting material contains homogeneous domains that are 10–100 μm on a side, and whose orientation is determined by that of the nanoscale seeds.

The concept of nanotube seeding of LCP domains is based on binary rod mixtures as theoretical models for liquid crystalline blends and composites. Liquid-crystalline molecules or supramolecular arrangements of molecules can be modeled as rigid rods, and LC phase behavior can be predicted solely on the basis of this model.¹¹ In addition,

the molecular rods will undergo spontaneous local alignment in the direction of larger rodlike objects if the diameters of the objects are commensurate.^{12,13} As a result, local coaxial alignment should occur between liquid-crystalline molecules and nanorods (such as SWNTs). Following this principle, Lynch and Patrick have aligned nematic, small-molecule LCs in an electric field and used these matrices to orient suspended SWNTs.¹⁴ We report that the converse effect can also be observed: SWNTs can be used to organize LCPs, via kinetic seeding of homogeneous liquid crystal domains from an LCP melt. We anticipate that this kinetic alignment approach will lead to the controlled alignment of bulk liquid crystalline material by orienting the SWNTs prior to the formation of the liquid crystalline phase.

The poly(oxazoline) **1**^{15–17} was selected as a model LCP for several reasons. First, the morphology of LCPs **1** can be controlled by varying the structure of side chains R (Figure 1). For example, for R = C₁₀H₂₁ (**1a**), columnar (ϕ_h , $p6mm$) LC phases are observed between approximately 60 and 100 °C for all polymer molecular weights.¹⁸ On the other hand, for R = C₁₅H₃₁ (**1b**), cubic ($Pm\bar{3}n$) LC phases predominate at low molecular weights (Figure 1).¹⁹ Percec has theorized that differences in the condensed-phase behavior of polymers **1** are dictated solely by steric interactions of the side chains.¹⁹ As a result, we have used this model polymer system as a way of examining the specific effect of SWNTs on LC phase behavior without varying the chemical composition of the polymer. Additionally, we presumed that oligoamide **1** might wrap around SWNTs, as has been reported for other

* Corresponding author. E-mail: taton@chem.umn.edu

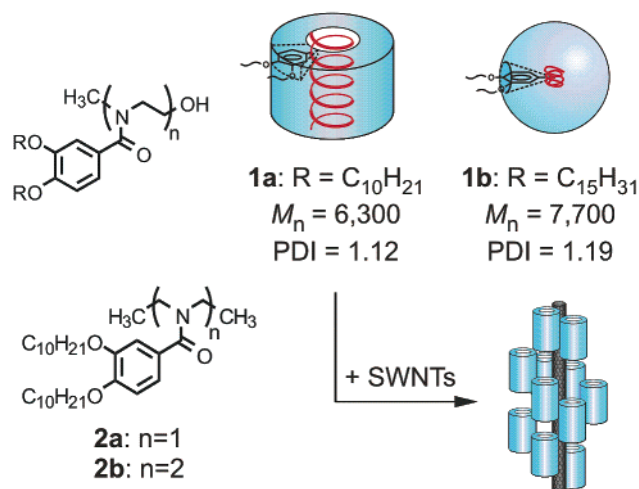


Figure 1. Structure and morphology of poly(oxazoline) liquid crystals (**1**) and model monomer and dimer (**2**).

polymers.^{20–23} Finally, polymers **1** were readily synthesized via ring-opening polymerization of mesogen-substituted oxazoline monomers, which allowed for different chemical functionalities or chain lengths to be conveniently introduced into the polymer.¹⁸

Poly(oxazolines) **1a** and **1b** were synthesized by the method of Percec and co-workers¹⁸ with minor modifications,²⁵ and exhibited physical properties consistent with those previously reported.¹⁸ We found that polymers **1** were effective at aiding the suspension of SWNTs in organic solvents, as has been described for other polymer systems.^{20–23} For example, while the solubility of SWNTs in diethyl ether (Et₂O) is negligibly low, a concentrated suspension of SWNTs in Et₂O could be obtained by adding 0.5 mg of solid SWNT material (Carbon Nanotechnologies, Houston, TX; $d = 0.79–1.1$ nm; $l = 1–5$ μm) and 20 mg of **1** to 10 mL of Et₂O, sonicating for 60 min, and filtering through cotton. After repetitive filtration, a stable, translucent, black suspension of up to 0.38 wt % SWNTs was achieved in Et₂O.²⁴ Stable SWNT suspensions could also be obtained with **1** in THF, benzene, and CHCl₃. Interestingly, the poly(oxazoline)–SWNT mixture (**1**·SWNT) could be homogeneously dispersed in some solvents that dissolve neither the polymer nor SWNTs alone. For example, **1a** by itself produces a cloudy suspension in benzene or Et₂O, but addition of SWNTs to this suspension clarifies the mixture and reduces the total optical extinction at visible wavelengths (as measured by UV–vis spectroscopy²⁴) due to decreased scattering. Although this behavior is consistent with a structural model of polymer **1a** wrapped around individual SWNTs or SWNT bundles, with solubilizing alkyl chains directed outward into solution, we currently have no experimental proof of this geometrical relationship between **1a** and SWNTs.

The polymeric structure of **1** was essential to stabilizing SWNT suspensions, as evidenced by the fact that neither monomer **2a** nor dimer **2b** was capable of solubilizing SWNTs. However, both **1a** and **1b** formed stable SWNT suspensions, indicating that the condensed-phase, LC structure of **1** does not necessarily dictate the structural interaction

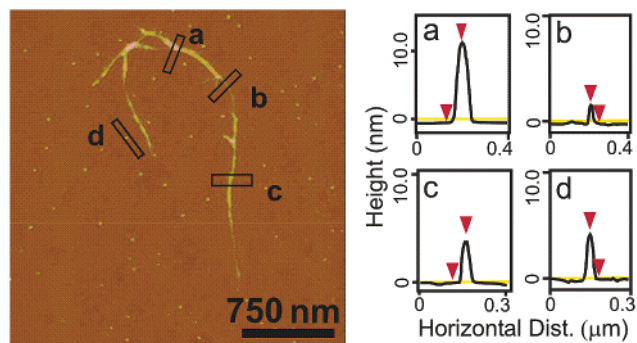


Figure 2. AFM image of **1a**·SWNT deposited from THF onto freshly cleaved mica. Samples were prepared by diluting the solid composite material with THF to a concentration of 10^{−4} g/mL (**1a**·SWNT containing 0.38 wt % SWNTs), and then spin-coating onto a freshly cleaved mica surface. Images were obtained in tapping mode on a Nanoscope III (Digital Instruments, Santa Barbara, CA) instrument. Cross sectional heights (averaged across the short axis of each section): **a**, 11.8 nm; **b**, 1.8 nm; **c**, 3.8 nm; **d**, 4.0 nm.

between the polymer and SWNTs in solution. To better characterize the structural interaction between the polymer and SWNTs, dispersed **1a**·SWNT was deposited onto freshly cleaved mica and imaged by atomic force microscopy (AFM). The images indicate that the SWNTs are dispersed as individual tubes rather than bundles and that the tubes are not completely covered by polymer (Figure 2). Some regions of the deposited nanotubes show heights of 1.8 nm or less, which is consistent with a single, bare SWNT. Other regions are thicker, with heights ranging from 4 to 12 nm, indicating the objects are either single or multiple SWNTs coated with polymer. Percec and co-workers have estimated the diameter of a single helical column of polymer **1a** to be 3.4 nm in the condensed phase, based on small-angle X-ray scattering measurements.¹⁸ As a result, the thicker segments of nanotube are likely associated with molecules of **1a**, though the AFM images do not indicate whether the polymer is helically wrapped around the tubes. Significantly less polymer material was found on other areas of the mica substrate than was bound to the SWNTs, which confirms the affinity of **1a** for the nanotube walls. The weight ratio of polymer to nanotubes deposited onto the sample was greater than 200:1, which we estimate to be more than sufficient to coat the entire nanotube surface in the sample with polymer.²⁵ The bare nanotube surface may result from an equilibrium between free and bound chains of **1a**, which has been used to explain why other interacting polymer systems must be in considerable excess in order to disperse SWNTs.²²

The solvent could be evaporated from suspensions of **1a**·SWNT to yield a gray, waxy composite solid that was optically clear and qualitatively stiffer than pure **1a**. By contrast, concentrated **1b**·SWNT was unstable and segregated into clear **1b** and black nanotube aggregates. We suggest that the SWNTs are dispersed poorly into **1b** because the SWNT rods are not accommodated by the cubic (spherical micellar) morphology of the polymer. As expected, the physical properties of stable **1a**·SWNT composites were substantially different from those of **1a** alone, for a wide

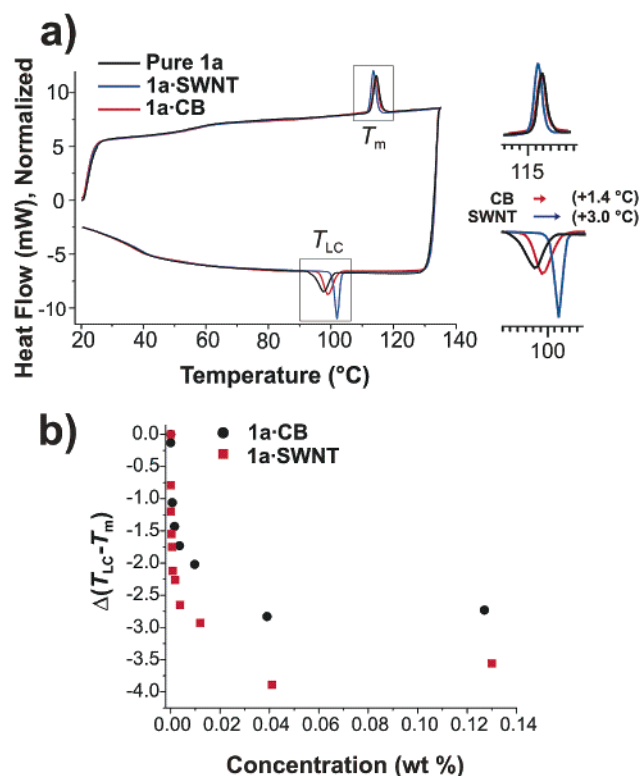


Figure 3. (a) DSC traces of **1a**, **1a**·SWNT containing 1.6×10^{-3} wt % SWNTs, and **1a**·CB containing 1.8×10^{-3} wt % carbon black. **1a**·SWNT and **1a**·CB both exhibit a shift in the T_{LC} to higher temperatures. (b) Change in the undercooling with increasing concentration of SWNTs and CB. Undercooling is defined as $(T_{LC} - T_m)$.

range of molecular weights ($M_n = 3,100$ to $8,100$ g/mol). Composites formed between **1a** with $M_n = 6,300$ g/mol and different weight fractions of SWNTs were chosen to characterize these differences in detail.²⁵ We found that polymer **1a** with $M_n = 6,300$ g/mol yielded sharp thermal transitions by differential scanning calorimetry (DSC) and large, reproducible textures by polarized light microscopy (PLM). However, the differences between **1a** and **1a**·SWNT described below were also observed qualitatively for other molecular weights. As expected, the thermal transitions and optical textures of **1b** were not affected by the presence of poorly dispersed SWNT aggregates.

Although we anticipated that the affinity of **1a** for nanotube walls would affect phase transitions in the composite material, it was not clear whether that effect would be thermodynamic, kinetic, or both. DSC analysis of pure **1a** and **1a**·SWNT composite containing 0.0016 wt % SWNTs (Figure 3a) showed both second-order transitions between the glass and LC phases (broad, near 55°C) and first-order transitions between the LC and isotropic phases (sharper, above 95°C). Importantly, dispersed SWNTs had no significant effect on the melting temperature ($T_{LC \rightarrow I}$, or T_m) of **1a**, but had a dramatic effect on the reverse transition temperature at which the liquid crystalline phase was reformed ($T_{I \rightarrow LC}$, or T_{LC}). This observation is consistent with a kinetic effect of SWNTs, in which nanotubes seed the formation of liquid crystalline domains from the melt.

Nucleation theory predicts that solid seeds or heterogeneous impurities should influence the observed T_c of a material but not its T_m .²⁶ Previous research has demonstrated that nucleation theory similarly applies to the T_{LC} of liquid crystals.^{27–29} To test whether SWNTs had a unique nucleating influence, spherical carbon black particles (Raven 7000, Columbian Chemicals; average particle diameter 11 nm) were also dispersed in **1a**,³⁰ and the resulting **1a**·CB composite material was analyzed by DSC. Again T_{LC} increased, albeit to a lesser extent than for **1a**·SWNT, and T_m remained the same. Both carbon black and SWNTs also caused a sharpening of the exothermic (T_{LC}) peak, with the effect of SWNTs being greater. In both cases, the undercooling, defined as $(T_{LC} - T_m)$, was minimized (i.e., the kinetic seeding effect was maximized) at fairly low weight fractions (<0.04 wt %) of added solid (Figure 3b). The plateau in the graph of $\Delta(T_{LC} - T_m)$ versus added solid is consistent with kinetic nucleation theory,³¹ which describes a maximum number of nuclei (N_m) above which the rate of phase transition is limited by phase growth rather than seeding. Over the range of 0–0.04 wt % SWNTs, where T_{LC} varies with added solid, the liquid-crystalline phase transition is kinetically controlled by the number of seeds.

Although SWNTs and carbon black had similar effects on the thermal properties of **1a**, the complementary, cylindrical architectures of SWNTs and **1a** have a more profound effect on the alignment and morphology of the LC phase. The birefringence of liquid crystalline **1a** allowed for easy observation of the growing LC domains using polarized light microscopy. Approximately 1 mg of **1a**, **1a**·SWNT, or **1a**·CB material was placed between sandwiched glass slides separated by $12.5\ \mu\text{m}$ -thick Teflon film spacers. These samples were then mounted on a polarizing microscope in a thermal heating block, heated to 120°C (well above T_{LC}), and then cooled at $0.5^\circ\text{C}/\text{min}$. Transmission-mode microscope images were captured every 10 s. Selected images of the cooling process are shown in Figure 4.³²

Below T_{LC} , liquid crystalline domains of pure **1a** grow radially as spherulites or striated fans, which produce clearly visible textures by polarized light microscopy (Figure 4A). Variation in the orientation of the local LC director is observed as light and dark regions in the image. In **1a**, this radial variation was confirmed by rotating the angle of the polarizer and watching the rotation of the extinction positions of individual fans. Spherulitic crystallite domain growth is typical for many crystalline polymers,³³ and was previously described for **1a**.¹⁸ Domains in **1a**·SWNT, on the other hand, grow homogeneously as spheroids from nucleation points in the material (Figure 4B). No striations are visible within the individual spheroids, indicating that there is a singular molecular orientation within each domain.³⁴ Consistent with this observation, rotating the polarizer 45° caused uniform changes in the extinction of all of the spheroids, indicating uniform director alignment within each domain. This behavior was observed at all points in the domain growth process. Eventually, the domains grew into each other as the phase transition completed to produce polydomain material with distinct LC domain boundaries. We hypothesize

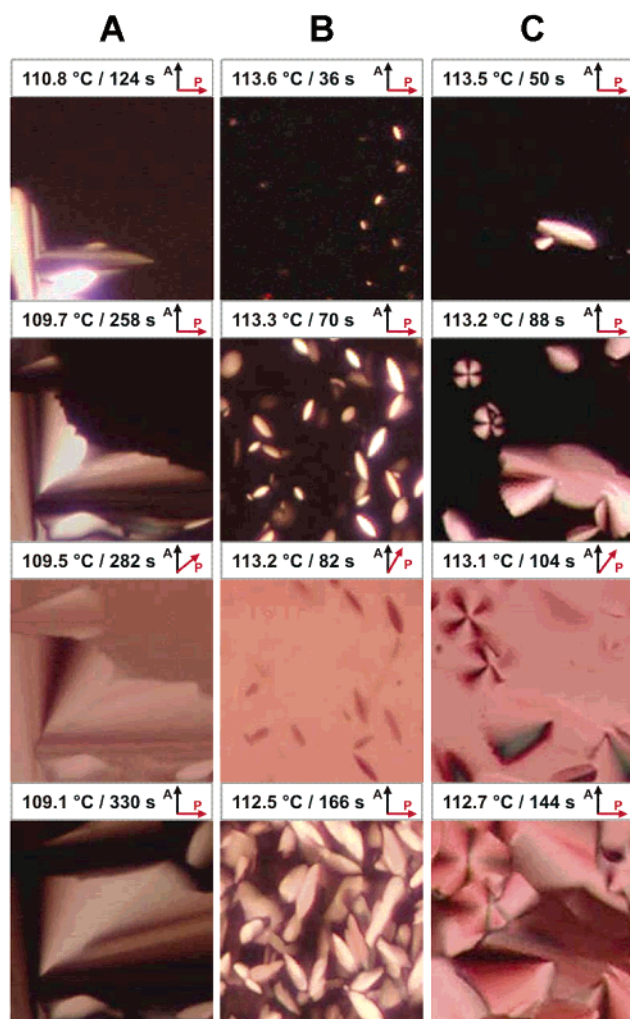


Figure 4. Polarized light microscope (PLM) images of pure **1a** (column A), **1a**-SWNT containing 1.5×10^{-4} wt % SWNT (column B), and **1a**-CB containing 2.3×10^{-4} wt % carbon black (column C). For each sample, images were obtained as the material was cooled from the isotropic melt at a rate of $0.5 \text{ }^\circ\text{C}/\text{min}$. The angles of the polarizer (P) and analyzer (A) are indicated above each image. For the first, second, and fourth images in each series, $\theta_{PA} = 90^\circ$; this angle has been reduced in the third image in each series to illustrate domain homogeneity. Each image measures $100 \text{ } \mu\text{m} \times 100 \text{ } \mu\text{m}$.³²

that LC domains in **1a**-SWNT are seeded by individual SWNTs or SWNT bundles, and that the orientation of each domain is determined by the orientation of its nanotube seed. By contrast, while **1a**-CB also exhibited seeded domain growth, the domains formed were spherulitic or fan-shaped as had been observed for pure **1a** (Figure 4C). We propose that homogeneous growth is not observed in **1a**-CB because of the structural mismatch between the cylindrical-phase liquid crystal and the spherical carbon particles.

Repeated melting and recooling of a sample of **1a**-SWNT past T_{LC} resulted in domain formation at the same locations (Figure 5a,b), demonstrating that the same seeds were kinetically active in each cooling cycle. Interestingly, the orientation of each domain varied slightly with each round of heating and cooling. This observation confirms that domains were not adventitiously nucleated by surface

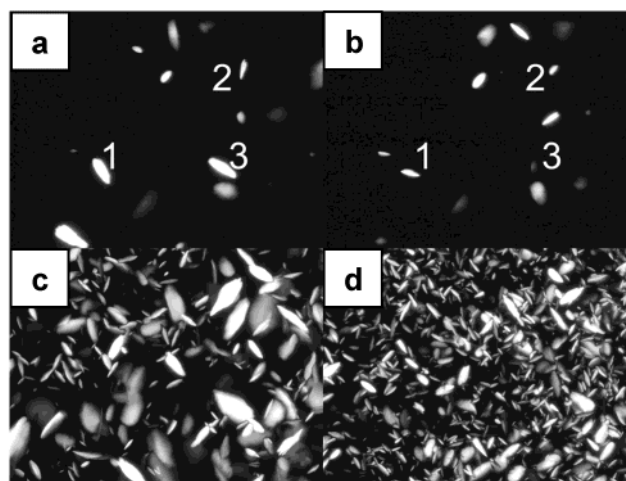


Figure 5. PLM images of identical regions of the same **1a**-SWNT sample (containing 3.7×10^{-4} wt % SWNTs) cooled at (a–b) $0.1 \text{ }^\circ\text{C}/\text{min}$, (c) $0.5 \text{ }^\circ\text{C}/\text{min}$, and (d) $1.5 \text{ }^\circ\text{C}/\text{min}$. After the cooling experiment in image (a), the sample was heated above T_m for 5 min and cooled at the same rate, resulting in reformation of the texture shown in image (b). Selected images were taken at approximately the same elapsed time (60 s) after initial texture formation. Each image measures $375 \text{ } \mu\text{m} \times 500 \text{ } \mu\text{m}$.

features on the microscope slides, but rather by freely rotating objects in suspension. The degree of rotation was presumably small because the high aspect ratio of SWNTs gives them small rotary diffusion coefficients in the viscous polymer melt.³⁵ Furthermore, the number of visible nuclei increased as the cooling was accelerated (Figure 5c,d), consistent with a progressive kinetic model of nucleation in which some seeds are inherently more active than others. It is important to note that, given the average length and diameter of the nanotubes and assuming that they are individually dispersed, we estimate²⁵ that there are more than 1×10^6 SWNTs in the imaged areas in Figure 5, which is far more than the number of seeds observed at even the fastest cooling rate. Clearly, only a few SWNTs or SWNT bundles are acting as nuclei in the homogeneous nucleation of **1a**-SWNT. We presume that the faster-growing, long axis of each spheroidal domain corresponds to the columnar axis of the liquid crystalline molecules, as has been previously characterized for fan-shaped textures in pure **1a**.¹⁶ If cooling was arrested immediately after domain growth began, longer, needle-shaped domains grew from each seed (Figure 6). This pattern of domain growth is consistent with both theoretical models^{12,13} and experimental observations¹⁴ of liquid crystal alignment on nanorods, in which liquid crystal molecules locally align in the direction of the templating rod. Local molecular organization then seeds the growth of larger, micron-sized LCP domains in **1a**. As a result, we argue that the orientation of liquid crystalline domains in **1a**-SWNT are determined exclusively by the shape and direction of the dispersed nanotubes.

In conclusion, we have demonstrated that SWNTs seed the growth of homogeneously ordered liquid crystalline domains in a model LCP. This model system allowed us to characterize the basic kinetic effects of nanoscale rods on a polymer mesophase, and confirmed theoretical predictions

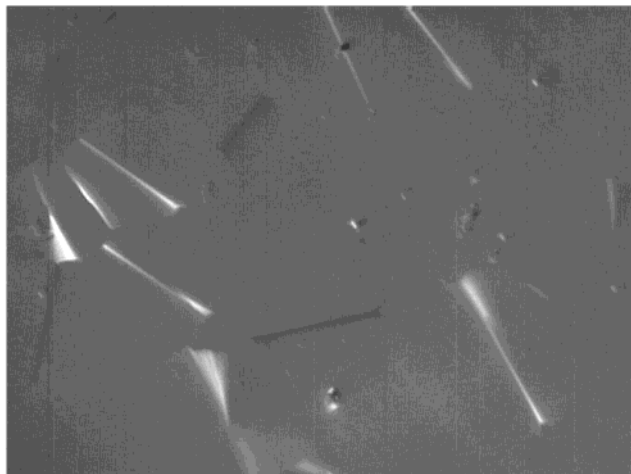


Figure 6. PLM image of **1a**-SWNT containing 1.6×10^{-4} wt % SWNT, ($M_n(\mathbf{1a}) = 8,000$ g/mol), in which cooling from the isotropic melt was arrested at the onset of texture formation. The image was taken with $\theta_{PA} = 90^\circ$ and an additional $\lambda/10$ Brace-Köhler compensator, which increases texture contrast and makes isotropic material appear gray rather than black. Sample thickness was controlled using $30 \mu\text{m}$ glass bead spacers (Polysciences Inc., Warrington, PA). The image measures $375 \mu\text{m} \times 500 \mu\text{m}$.³²

on the interactions between nanoscale rods and liquid crystal phases. We anticipate that, as long as seeding is determined by the fundamental interactions between liquid crystalline molecules and nanorods, the aligning effect of nanorods may be applied to other liquid crystalline polymer systems in which SWNTs can be stably dispersed. We are currently investigating the homogeneous alignment of bulk LCP–nanotube composite materials by preorienting the SWNT seeds prior to cooling the isotropic phase. The ease with which SWNTs are oriented by applied electric or magnetic fields^{36,37} or by shear flow^{38,39} makes SWNT-templated growth a particularly attractive approach to programming the organization of extruded, molded, or cast LCP forms. Because very small quantities of nanotubes were required to induce the domain growth and alignment observed in this study, we expect that kinetic seeding can be used to offset the relatively high cost of SWNTs and increase the potential for nanotube alignment to be used in technologically relevant materials.

Acknowledgment. This work was supported by the Research Corporation (Research Innovation Award RI0964) and the University of Minnesota.

Supporting Information Available: Detailed synthesis and characterization data for molecules **1** and **2**, concentration determinations of SWNTs and CB in solutions of **1**, details of temperature-controlled polarized light microscopy experiments, determination of specific absorptivity of carbon black, calculations of polymer coverage and SWNTs in the viewing area, and domain growth movies. This material is available free of charge via the Internet at <http://pubs.acs.org>.

References

- (1) *Thermotropic Liquid Crystal Polymers: Thin-Film Polymerization, Characterization, Blends, and Applications*; Chung, T.-s., Ed.; Technomic: Lancaster, 2001.

- (2) Donald, A. M.; Windle, A. H. *Liquid Crystalline Polymers*; Cambridge University Press: Cambridge, UK, 1992.
- (3) *Rheology and Processing of Liquid Crystal Polymers*; Acierino, D.; Collyer, A. A., Eds.; Chapman & Hall: London, New York, 1996.
- (4) Yoon, H. N.; Charbonneau, L. F.; Calundann, G. W. *Adv. Mater.* **1992**, *4*, 206–214.
- (5) Zakharov, A. V.; Dong, R. Y. *Phys. Rev. E* **2002**, *65*, 052701.
- (6) Iverson, I. K.; Casey, S. M.; Seo, W.; Tam-Chang, S.-W.; Pindzola, B. A. *Langmuir* **2002**, *18*, 3510–3516.
- (7) *Liquid Crystals: Experimental Study of Physical Properties and Phase Transitions*; Kumar, S., Ed.; Cambridge University: Cambridge, 2001.
- (8) Anwer, A.; Windle, A. H. *Polymer* **1991**, *32*, 103–108.
- (9) Kanel, H. V.; Litster, J. D.; Melngailis, J.; Smith, H. I. *Phys. Rev. A* **1981**, *24*, 2713–2719.
- (10) Berreman, D. W. *Phys. Rev. Lett.* **1972**, *28*, 1683–1686.
- (11) Onsager, L. *Ann. N. Y. Acad. Sci.* **1949**, *51*, 627–659.
- (12) Sear, R. P.; Mulder, B. M. *J. Chem. Phys.* **1997**, *106*, 3827.
- (13) van Roij, R.; Mulder, B. *Phys. Rev. E* **1996**, *54*, 6430–6440.
- (14) Lynch, M. D.; Patrick, D. L. *Nano Lett.* **2002**, *2*, 1197–1201.
- (15) Ungar, G.; Abramic, D.; Percec, V.; Heck, J. A. *Liq. Cryst.* **1996**, *21*, 73–86.
- (16) Seitz, M.; Plesniviy, T.; Schimossek, K.; Edelmann, M.; Ringsdorf, H.; Fischer, H.; Uyama, H.; Kobayashi, S. *Macromolecules* **1996**, *29*, 6560–6574.
- (17) Stebani, U.; Lattermann, G.; Festag, R.; Wittenberg, M.; Wendorff, J. H. *J. Mater. Chem.* **1995**, *5*, 2247–2251.
- (18) Percec, V.; Holerca, M. N.; Magonov, S. N.; Yearley, D. J. P.; Ungar, G.; Duan, H.; Hudson, S. D. *Biomacromolecules* **2001**, *2*, 706–728.
- (19) Percec, V.; Holerca, M. N.; Uchida, S.; Yearley, D. J. P.; Ungar, G. *Biomacromolecules* **2001**, *2*, 729–740.
- (20) Czerw, R.; Guo, Z.; Ajayan, P. M.; Sun, Y.-P.; Carroll, D. L. *Nano Lett.* **2001**, *1*, 423–427.
- (21) O’Connell, M. J.; Boul, P.; Ericson, L. M.; Huffman, C.; Wang, Y. H.; Haroz, E.; Kuper, C.; Tour, J.; Ausman, K. D.; Smalley, R. E. *Chem. Phys. Lett.* **2001**, *342*, 265–271.
- (22) Star, A.; Stoddart, J. F.; Steuerman, D.; Diehl, M.; Boukai, A.; Wong, E. W.; Yang, X.; Chung, S. W.; Choi, H.; Heath, J. R. *Angew. Chem., Int. Ed. Engl.* **2001**, *40*, 1721–1725.
- (23) Star, A.; Steuerman, D. W.; Heath, J. R.; Stoddart, J. F. *Angew. Chem., Int. Ed. Engl.* **2002**, *41*, 2508–2512.
- (24) Weight fractions of SWNTs in suspensions were determined using the reported specific absorptivity of $0.0286 \text{ L mg}^{-1} \text{ cm}^{-1}$ (Bahr, J. L. et al., *Chem. Commun.* **2001**, 193–194). See Supporting Information for details.
- (25) See Supporting Material for experimental details.
- (26) Ozawa, T. *Polymer* **1971**, *12*, 150–158.
- (27) Jabarin, S. A.; Stein, R. S. *J. Phys. Chem.* **1973**, *77*, 409–413.
- (28) Liu, X.; Hu, S.; Shi, L.; Xu, M.; Zhou, Q.; Duan, X. *Polymer* **1989**, *30*, 273–279.
- (29) Armitage, D.; Price, F. P. *Mol. Cryst. Liq. Cryst.* **1978**, *44*, 33–44.
- (30) Carbon black weight fractions were determined using the specific absorptivity of $0.0103 \text{ L mg}^{-1} \text{ cm}^{-1}$. See Supporting Information for more details.
- (31) Kashchiev, D. *Nucleation: Basic Theory with Applications*; Butterworth Heinemann, 2000.
- (32) Complete movie sequences are available free of charge via the Internet at <http://pubs.acs.org>.
- (33) Schultz, J. M. *Polymer Crystallization: The Development of Crystalline Order in Thermoplastic Polymers*; Oxford University: New York, 2001.
- (34) Neubert, M. In *Liquid Crystals: Experimental Study of Physical Properties and Phase Transitions*; Kumar, S., Ed.; Cambridge University: Cambridge, 2001.
- (35) Larson, R. G. *The Structure and Rheology of Complex Fluids*; Oxford University: New York, 1999.
- (36) Smith, B. W.; Benes, Z.; Luzzi, D. E.; Fischer, J. E.; Walters, D. A.; Casavant, M. J.; Schmidt, J.; Smalley, R. E. *Appl. Phys. Lett.* **2000**, *77*, 663–665.
- (37) Diehl, M. R.; Yaliraki, S. N.; Beckman, R. A.; Barahona, M.; Heath, J. R. *Angew. Chem., Int. Ed. Engl.* **2001**, *41*, 353–356.
- (38) Haggmueller, R.; Gommans, H. H.; Rinzler, A. G.; Fischer, J. E.; Winey, K. I. *Chem. Phys. Lett.* **2000**, *330*, 219–225.
- (39) Vigolo, B.; Penicaud, A.; Coulon, C.; Sauder, C.; Pailler, R.; Journet, C.; Bernier, P.; Poulin, P. *Science* **2000**, *290*, 1331–1334.

NL0347738